Marine Chemistry
January 2023, Volume 248, Pages 104207 (10 p.)
https://doi.org/10.1016/j.marchem.2023.104207
https://archimer.ifremer.fr/doc/00815/92667/

The distribution of ^{227}Ac along the GA01 section in the North Atlantic

Le Roy Emilie [1, 2, *], Van Beek Pieter [1], Lacan François [1], Souhaut Marc [1], Sanial Virginie [3], Charette Matthew A. [2], Henderson Paul B. [2], Deng Feifei [4]

[1] LEGOS, Laboratoire d'Etudes en Géophysique et Océanographie Spatiales (Université de Toulouse, CNRS/CNES/IRD/UPS), Observatoire Midi Pyrénées, 14 Avenue Edouard Belin, 31400 Toulouse, France
[2] Department of Marine Chemistry and Geochemistry, Woods Hole Oceanographic Institution, Woods Hole, MA 02543, USA
[3] Univ Toulon, Mediterranean Institute of Oceanography, Aix Marseille Univ., CNRS/INSU, IRD, UM 110, Université de Toulon laboratoire MIO CS 60584, 83041 Toulon, France
[4] Institute of Coastal Research, Helmholtz-Zentrum Geesthacht Center for Materials and Coastal Research, Max-Planck Str.1, 21502 Geethacht, Germany

* Corresponding author : Emilie Le Roy, email address : emilie.leroy@univ-brest.fr

Abstract :

Actinium-227 is a powerful tool to study vertical mixing in the ocean, and was more recently proposed as a tracer of hydrothermal plumes. However, because 227Ac activities are especially low in the ocean, relatively few studies have been conducted to date, and none has been done on the large scale, as is reported in the present study. Here, we report a section of dissolved 227Ac in the North Atlantic Ocean between Portugal-Greenland-Canada based on nine full-depth profiles obtained in the framework of the international GEOTRACES program (GA01 section - GEOVIDE cruise, May–July 2014). The simultaneous determination of 231Pa, the parent nuclide of 227Ac, along the section allowed us to report a section of excess 227Ac activities (227Acex).

Actinium-227 activities were especially low along the section (<0.4 dpm m−3) compared to other ocean basins. In most cases, 227Ac activities reached secular equilibrium with 231Pa in the water column 500 m above the seafloor. Secular equilibrium is considered reached after ~five half-lives of the daughter. Secular equilibrium therefore suggests no external input over the last ~100 years. The highest 227Ac activities were often found close to the seafloor, indicating that 227Ac diffuses out of the sediments. However, two different patterns question the traditional one-dimensional vertical mixing model typically applied to 227Ac released by deep-sea sediments: first, significant 227Acex were found in the upper 500 m of the water column at several stations located near the Iberian margin. In the upper 500 m, the high 227Acex activities could indicate lateral advection of waters that interacted with the margins. Second, mid-water peaks of 227Acex were occasionally observed along the transect. At station 44 in the Irminger Basin, a peak of 227Acex activity at 2500 m that was co-located with high dissolved Fe concentrations could be interpreted as the signature of a hydrothermal plume. Near the seafloor, we often observed bottom nepheloid layers and we cannot exclude that these layers impact the 227Ac distributions.

Highlights

► Actinium-227 activities were especially low along the section (<0.4 dpm m^{-3}) compared to other ocean basins. ► In most cases, ^{227}Ac activities reached secular equilibrium with ^{231}Pa (suggesting no external input over the last ~100 years) in the water column 500 m above the seafloor. ► The highest ^{227}Ac activities were often found close to the seafloor, indicating that ^{227}Ac diffuses out of the sediments. ► In the upper 500 m, high $^{227}Ac_{ex}$ activities could indicate lateral advection of waters that interacted with the margins. ► Near the seafloor, we often observed bottom nepheloid layers and we cannot exclude that these layers impact the ^{227}Ac distributions, since manganese oxides were shown to be present in these layers and may thus scavenge ^{227}Ac among other radionuclides.+

Keywords : GEOTRACES, Actinium, Actinium-227, North Atlantic

1. Introduction

Actinium-227 (^{227}Ac) is a deep-sea mixing tracer that combines the advantages of a source in the deep-sea sediments with a half-life of 21.8 y. ^{227}Ac is produced by the decay of its parent nuclide protactinium-231 (^{231}Pa; $T_{1/2}$ = 32 760 y), ^{231}Pa being itself produced following the decay of uranium-235 (^{235}U; $T_{1/2}$ = 7.04 10^8 y). ^{235}U activities in the ocean are mostly constant through space and time due to its long residence time (~0.5 Ma; Ku et al., 1977), which leads to a uniform production rate of ^{231}Pa in the water column. Once produced, ^{231}Pa rapidly adsorbs onto particles. It is then transported to the seafloor and thus, accumulates slowly in the sediments (Anderson et al., 1983). In the sediment, ^{231}Pa decays to ^{227}Ac which is then released to the overlying water column due to its higher solubility (Anderson et al., 1983; Nozaki, 1984; Nozaki et al., 1990; Nozaki, 1993, p.199; Geibert et al., 2002; Kemnitz et al., 2022). ^{227}Ac that diffuses out of the sediments is then redistributed in the ocean by transport (advection and upwelling) and mixing (Nozaki, 1984; Geibert et al., 2002; Koch-Larrouy et al., 2015). The ^{227}Ac that diffuses out of the sediment thus adds to the ^{227}Ac produced in the water column (from ^{231}Pa) that is considered to be at secular equilibrium with ^{231}Pa, assuming steady-state conditions (Nozaki, 1984). Excess ^{227}Ac activities ($^{227}Ac_{ex}$, the difference between the total activities and ^{227}Ac at secular equilibrium with ^{231}Pa) are thus often observed up to ca. 500 m above the seafloor due to vertical mixing (Geibert et al., 2002; Nozaki, 1984). Nozaki (1984) proposed estimating vertical eddy diffusivity coefficients (K_z) from the $^{227}Ac_{ex}$ vertical distribution. $^{227}Ac_{ex}$ has also been used to estimate upwelling rates, since this process also brings ^{227}Ac toward the surface (Geibert et al., 2002; Haskell et al., 2015; Kemnitz et al., 2022). Finally, Kipp et al. (2015) showed that hydrothermal vents constituted a source of ^{227}Ac to the deep Atlantic Ocean that was equivalent to ~2-6% of the deep-sea sediment flux.

^{227}Ac concentration in the ocean is, however, especially low. Its global oceanic inventory is only 37 mol or 8.4 kg (Geibert et al., 2008). In addition, interpretation of its distribution requires the knowledge of its ^{231}Pa parent distribution. As a result, the use of dissolved excess ^{227}Ac as an oceanic tracer has been reported in few studies to date (Dulaiova et al., 2012; Geibert et al., 2008, 2002; Geibert and Vöge, 2008; Kipp et al., 2015; Le Roy et al., 2019; Koch-Larrouy et al., 2015; Nozaki, 1984, 1993; Nozaki et al., 1990; Levier et al., 2021; Kemnitz et al., 2022). In the present study, we report nine vertical profiles of ^{227}Ac from a large-scale section in the North Atlantic Ocean and the Labrador Sea.

Th[illegible] al., 2018). The determination of both ^{227}Ac and ^{231}Pa at the nine full-depth vertical profiles provides a unique section of $^{227}Ac_{ex}$ activities in the North Atlantic.

2. Material and Methods

2.1. GEOVIDE Cruise

The GEOVIDE section (GEOTRACES GA01; PIs: Géraldine Sarthou, LEMAR, France and Pascale Lherminier, LOPS, France) was conducted in the North Atlantic Ocean between Lisbon, Portugal and St John's, Newfoundland on board the R/V *Pourquoi Pas?* (15 May 2014-30 June 2014; Fig.1). The section crossed different topographic features and regions displaying contrasting biogeochemical patterns. It complements sections GA03 and GA02 also conducted in the Atlantic Ocean in the framework of the GEOTRACES program.

2.2. Hydrodynamic Context

An Optimum Multiparameter Analysis (OMPA) was used to estimate the contributions of the different water masses found along the GEOVIDE section (García-Ibáñez et al., 2018). First, Central Waters, carried by the North Atlantic Current (NAC), occupy the upper eastern part of the GEOVIDE section from the Iberian Peninsula to the Rockall Trough (stations 1 to 26; Fig.2). Part of the Central Waters flows toward the Iceland Basin and the Irminger Sea and forms the Iceland Subpolar Mode Water (IcSPMW) in the Iceland Basin over the Reykjanes Ridges. Then, these waters follow the Irminger Current (Stations 32 and 38; Fig.2; Lacan and Jeandel, 2005; McCartney, 1992). Then, the Irminger Subpolar Mode Water (IrSPMW) results from the transformation of the Central Waters and the IcSPMW, northwest of the Irminger Sea (Krauss, 1995). The IrSPMW is located near Greenland (Fig.2) (García-Ibáñez et al., 2015; Lacan and Jeandel, 2004; Read, 2000). The Labrador Sea Water (LSW) is an intermediate water mass formed by deep winter convection in the Labrador Sea resulting from progressive cooling and freshening of surface waters (station 69;Lazier, 1973). It is observed at multiple locations along the GEOVIDE section. It flows northward into the Irminger Sea (station 44) and eastward across the Mid-Atlantic Ridge (MAR). It then splits northward into the Iceland Basin (station 32), eastward into the West European Basin (stations 21 and 26), and equatorward. The Mediterranean Water (MW) enters the North Atlantic through the Gibraltar Strait and flows northwestward (García-Ibáñez et al., 2015). The Iceland-Scotland Overflow Water (ISOW) originates at the Iceland-Scotland sill and entrains the overlying warm saline Atlantic waters (SPMW) and LSW (van Aken, 2000). ISOW was found at stations located on the Eastern flank of the Reykjanes Ridge (stations 32 and 38) and near Greenland (station 64) at great depth (2000–3500 m) (Fig.2). Slightly deeper, the overflow waters coming from the Denmark Strait Overflow Water (DSOW) are then

flo[illegible] the northern end of the Irminger Sea (station 44) and the deepest part of the Greenland continental slope (stations 69 and 77) (Fig.2). The Lower North East Atlantic Deep Water (NEADWl) is a water mass with a southern origin lying at the bottom of the West European Basin (stations 1 to 26 in Fig.2). It recirculates into the Rockall Trough and meets ISOW in the Iceland Basin (van Aken, 2000; McCartney, 1992; Schmitz and McCartney, 1993).

2.3. Sample collection

Due to the low ^{227}Ac activities in the ocean (<5 dpm m^{-3}, Geibert et al., 2002; 0.1 - 4.8 dpm m^{-3}, (Levier et al., 2021), the analysis of ^{227}Ac requires a pre-concentration step from large volumes of seawater. We used acrylic cartridges impregnated with manganese oxide (Mn-cartridges) mounted on large volume *in-situ* pumps, a method that is largely used to preconcentrate radionuclides from seawater such as Ra and Th isotopes, as well as ^{227}Ac (Henderson et al., 2013; Swarzenski and Baskaran, 2004). Pumps were deployed at 6 to 13 depths at each of the investigated stations. Pumping was carried out for 3 to 4 hours to filter large seawater volumes (420 to 1565 L). The resulting flow rates mostly ranged from 3 to 6 L min^{-1}. Seawater was first filtered *in situ* through Supor (Pall, 0.8 µm pore size) or QMA (Sartorius, 1 µm pore size, Ø 142 mm) membranes to collect suspended particles, and then through the cartridges impregnated with MnO_2 (Mn-cartridges) to collect dissolved ^{227}Ac (as well as Ra isotopes). For the deep samples, two Mn-cartridges (cartridge A and cartridge B) were placed in line to provide information on the yield of ^{227}Ac fixation onto the Mn-cartridges. Following collection, each Mn-cartridge was rinsed with Ra-free milli-Q water and slightly dried using compressed air. This protocol and the method used to determine the yield of ^{227}Ac fixation onto the Mn cartridges are presented in more detail in (Le Roy et al., 2019).

2.4. Quantification of the ^{227}Ac activities

Following Shaw and Moore (2002), we used Radium Delayed Coincidence Counters (RaDeCC, Scientific Computer Instruments, USA; Moore and Arnold, 1996) to quantify ^{227}Ac activities on the Mn-cartridges. The ^{223}Ra in equilibrium with ^{227}Ac was determined by measuring the ^{219}Rn activities that are in secular equilibrium with ^{223}Ra and ^{227}Ac. This method is extensively described in (Le Roy et al., 2019) and briefly summarized below. The partially dried Mn-cartridges were placed in plastic cartridge holders in a closed helium circulation loop. Helium was allowed to circulate through the Mn-cartridges and carried the ^{219}Rn to the scintillation cell coated with ZnS, where alpha particles produced by the ^{219}Rn decaying into ^{215}Po were detected. A delayed coincidence system (originally developed by (Giffin et al., 1963) and then adapted by Moore and Arnold, (1996) allowed us to discriminate the signal associated to ^{219}Rn from those of other Rn isotopes (^{220}Rn and ^{222}Rn) which were not associated with ^{227}Ac. Corrections for chance coincidence counts were performed following Moore and Arnold

(19[illegible] i.e. a Mn-cartridge containing a known amount of ^{227}Ac (Le Roy et al., 2019). Dissolved ^{227}Ac activities were then determined using the Mn-cartridge extraction efficiency determined from the two Mn cartridges placed in series (Le Roy et al., 2019). A mean extraction efficiency of 47 ± 12% was applied to all Mn-cartridges (1 SD, n=21; (Le Roy et al., 2019). Repeatability experiments allowed us to estimate the uncertainty associated with the ^{227}Ac analysis (19%, 1SD; Le Roy et al., 2019).

Excess ^{227}Ac activities ($^{227}Ac_{ex}$) were then calculated following:

$$^{227}Ac_{ex} = {}^{227}Ac - {}^{231}Pa \qquad \text{Equation (1)}$$

This is assuming that a fraction of the ^{227}Ac present in the water column is at secular equilibrium with ^{231}Pa. In some cases, the dissolved ^{231}Pa activities were collected using a separate sampling system and therefore not determined at the exact same water depth as the ^{227}Ac activities (Deng et al., 2018). We thus used the depth interpolated ^{231}Pa activity determined from samples collected above and below the ^{227}Ac sample.

3. Results

3.1. ^{227}Ac distribution along the GEOVIDE section

The distribution of ^{227}Ac activities along the GEOVIDE section is shown in figure 3. As a comparison, the ^{231}Pa activities are also reported (isolines). Most samples displayed activities ranging between 0.02 and 0.4 dpm m^{-3}, with higher ^{227}Ac activities observed in deep waters near the seafloor: deep waters at the bottom of the West European Basin and in the Irminger basin at 2500 m display ^{227}Ac activities of 0.6 and 1.1 dpm m^{-3}, respectively. In upper waters (~500 m), slightly higher activities can be found near the margins (e.g., stations 1 and 13 located on the Iberian margin or station 64 located near Greenland).

Excluding the enrichments observed in deep waters, ^{227}Ac activities determined along the section were in the lower range of the ^{227}Ac activities reported by Nozaki et al. (1998) in the northeast Pacific: 0.05 dpm m^{-3} in the upper water column to 2.68 dpm m^{-3} near the seafloor. However, the ^{227}Ac activities reported here were in the same order of magnitude as those reported by (Geibert et al., 2002) in the central Arctic (^{227}Ac activities ranging from 0.08 dpm m^{-3} at 1220 m to 0.28 dpm m^{-3} at 4220 m). In the Atlantic Ocean, (Kipp et al., 2015) reported ^{227}Ac activities as low as 0.16 dpm m^{-3} at 1060 m and up to 0.55 dpm m^{-3} at 4700 m; higher ^{227}Ac activities (up to 1.44 dpm m^{-3}) were associated with a neutrally buoyant hydrothermal vent plume.

3.2. ^{227}Ac vs ^{231}Pa activities and $^{227}Ac_{ex}$ distribution

In general, ^{227}Ac activities gradually increased with increasing depth at stations located in the West European Basin (stations 1, 13, 21 and 26; Fig. 4, Table 1). In contrast, the increase with depth was

vertical distribution of ^{231}Pa activities that increased with increasing depth in the West European basin from 0.04 dpm m^{-3} in the surface waters to 0.28 dpm m^{-3} in the deep waters (Deng et al., 2018). In contrast, a lower and narrower range of ^{231}Pa activities was observed in the Irminger and Labrador basins (0.05 - 0.15 dpm m^{-3}; (Deng et al., 2018). At intermediate depths (below ca. 500 m and above 500 m above the seafloor), ^{227}Ac and ^{231}Pa activities were similar for most of the investigated stations. This suggests that at these depths, ^{227}Ac originated from the decay of ^{231}Pa in the water column. However, at several intermediate depths, ^{227}Ac activities were slightly lower than ^{231}Pa (e.g., stations 13, 21, 38).

The $^{227}Ac_{ex}$ section is shown in Fig.5. The $^{227}Ac_{ex}$ distribution mirrors that of ^{227}Ac (Fig.3). Significant $^{227}Ac_{ex}$ activities were found at several stations near the seafloor (13, 26, 32, 44, 64 and 69), but this was not the case for all stations, with excess activities reaching up to 1.0 dpm m^{-3} (Fig.4 and 5). Occasional isolated peaks in $^{227}Ac_{ex}$ activities were found at depths away from the seafloor (station 44; 2500 m; stations 1 and 21; 500 m). Surprisingly, surface waters also sometimes exhibited significant $^{227}Ac_{ex}$ activities (stations 1, 13, 32, 44 and 64).

4. Discussion

4.1. Influence of the water masses on the ^{227}Ac distribution

^{227}Ac is at secular equilibrium with ^{231}Pa for most of the stations between 500 m below the surface and ca. 500 m above the seafloor, excluding the sporadic higher ^{227}Ac values that were sometimes observed in the water column (Fig.3). Indeed, $^{227}Ac_{ex}$ is in most cases relatively low when compared to other oceanic regions (Geibert et al., 2008, 2002; Nozaki, 1984; Levier et al., 2021). Water masses that display ^{227}Ac at secular equilibrium suggest that they did not enter in contact with sediments over the last 100 years (five ^{227}Ac half-life). East of the section, the vertical ^{231}Pa activities increase with increasing depth and may reflect reversible scavenging. In particular, the NEADWl, located in the eastern part of the section, has a southern component (Fig. 2). NEADWl, with an apparent age of at least 400 years, and is an old water mass (not recently ventilated) compared to the other water masses along the section that are less than 100 years old (Deng et al., 2018). NEADWl is thus characterized by relatively high ^{231}Pa activities, since ^{231}Pa activities increase with age (Deng et al., 2018). Consequently, the ^{227}Ac activities that are at secular equilibrium with ^{231}Pa also increase with increasing depth in the West European Basin (Fig.3).

In the western part of the section, the formation of deep-waters transports the low ^{231}Pa concentrations from surface waters into the deep ocean, where ^{231}Pa activities increase as the water mass is transported (Deng et al., 2018). In the Labrador and Irminger Basins, low ^{231}Pa (and thus ^{227}Ac) activities throughout the water column are thus explained by the presence of recently ventilated (young)

found in the Arctic Ocean, even close to the seafloor (Geibert et al., 2002).

4.2. $^{227}Ac_{ex}$ activities Near the Seafloor

The $^{227}Ac_{ex}$ activities increase near the seafloor at stations 13, 26, 32, 64 and 69 (Fig.5), but this pattern is not observed at all stations as would be expected from a tracer originating from deep-sea sediments. The highest $^{227}Ac_{ex}$ activity near the seafloor is found at station 13 (0.42 dpm m^{-3}), which is the deepest station investigated along the GEOVIDE section (5500 m). Since the accumulation rate of ^{231}Pa in sediments increases with increasing water column depth, the flux of ^{227}Ac diffusing out of the sediment is also a function of the water column thickness (Geibert et al., 2002). The same explanation holds for the three deep stations (13, 21, 26) located in the deep basins (Iberian Abyssal plain; West European basin) that display significant $^{227}Ac_{ex}$ activities near the seafloor. In addition, these stations are likely less impacted by advection and strong currents—since these basins are located away from boundary currents—than the other stations located west of the section. The ^{227}Ac enrichments near the seafloor are, however, restricted to the deep-sea and are rarely transported by vertical mixing further than 500 m above the seafloor (Fig. 4). This latter pattern contrasts with the profiles observed in the Pacific Ocean (Nozaki, 1984), where significant $^{227}Ac_{ex}$ activities can be found at a greater distance from the seafloor.

Several vertical profiles of $^{227}Ac_{ex}$ do not show an increase near the seafloor, where $^{227}Ac_{ex}$ activities are expected (Nozaki, 1984). Benthic nepheloid layers were observed along the GEOVIDE section from the Iceland basin to the Labrador Basin (Stations 26 to 69), as deduced from decreases in the transmissiometry near the seafloor, indicative of an increase in the particle concentration (Fig.4). These bottom nepheloid layers may impact the distribution of radionuclides in the dissolved phase. In particular, the particulate Mn concentrations (PMn) also increase near the seafloor within the bottom nepheloid layers at all these stations (Fig.4). PMn is well known to scavenge radionuclides, including radionuclides reactive to particles such as Th or Pa. Scavenging near the seafloor has been reported by previous studies in the Labrador Basin (Bacon and Anderson, 1982; Deng et al., 2014, 2018). This is potentially also the case for radionuclides such as Ra isotopes and ^{227}Ac, although this effect has never been investigated in past studies. It is the property of MnO_2 to adsorb radionuclides that has led to the use of fibers and cartridges impregnated with Mn to pre-concentrate radionuclides from seawater samples (Moore and Reid, 1973) and to co-p+recipitate Ra (Ghaleb et al., 2004) and Ac (Levier et al. 2021). Such impact, however, has never been clearly reported in oceanic studies. Some high manganese oxide concentrations are associated with particles resuspended from the sediment. However, we could not find, any statistical relationship between PMn concentrations and ^{227}Ac, ^{226}Ra and ^{231}Pa patterns near the seafloor (Fig.4). Moreover, it is unclear why ^{227}Ac would be preferentially scavenged compared to ^{231}Pa. One hypothesis would be that recent re-suspension of surface sediments, with high

this process may really impact the distribution of radionuclides such as Ra and Ac.

4.3. $^{227}Ac_{ex}$ Enrichments in the Water Column

In the Irminger and Labrador Basins, some higher $^{227}Ac_{ex}$ activities were observed in deep waters, at stations 64 and 69, or even more clearly at station 44. Peaks of $^{227}Ac_{ex}$ may be indicative of a recent (younger than ~ 100 years) contact of the water mass with ocean boundaries such as margins and deep sediments (Nozaki, 1984; Nozaki et al., 1990) or indicative of a hydrothermal plume (Kipp et al., 2015).

The highest $^{227}Ac_{ex}$ activities across the section (1.12 dpm m^{-3}) were observed at 2500 m at station 44 in association with high dissolved iron (DFe) concentrations—up to 2.5 nmol L^{-1}—between 2000 m and 2800 m (Fig.4; Tonnard et al., 2018). The DFe and ^{227}Ac patterns observed at depth at station 44 may be attributed to the signature of a hydrothermal plume. Although there is no additional supporting evidence for hydrothermal activity (e.g. no parallel δ^3He measurements were made), hydrothermal vents have been reported along the nearby Reykjanes Ridge (Le Roy et al., 2019). At station 64, a slight increase of DFe concentration—up to 2.1 nmol L^{-1}—was observed between 2000 and 3000 m (Fig.4). The high $^{227}Ac_{ex}$ activities observed at stations 64 and 69 in deep waters may be explained by lateral advection of waters that interacted with the margins. The Irminger and Labrador Basins are not as deep as West European Basin and the Iberian Abyssal Plain. Second, currents are also stronger in this area, with the onset of the Deep Western Boundary Current (DWBC). These features may foster interaction between the water masses and the sediments.

Slightly higher ^{227}Ac activities were found at stations near the Iberian margin, at 500 m (stations 1 and 21) and in the upper 500 m at station 13. This pattern is similar to that reported in the Central Arctic where an input from Siberian shelves was suspected (Geibert et al., 2002). A similar increase at 500 m in the ^{227}Ac activities has also been recently reported in a vertical profile in the Weddell Gyre (Levier et al., 2021). Such high $^{227}Ac_{ex}$ activities at relatively shallow depths may be explained by lateral advection of waters that interacted with shallow sediments. In coastal regions, boundary scavenging leads to preferential ^{231}Pa removal in areas of high particle flux and therefore accumulation of ^{231}Pa in margin sediments (Anderson et al., 1983; Bacon et al., 1976). However that flux maybe diluted by a higher detrital input than in deep waters. Another hypothesis is extensive irrigation of sediments by fauna that could produce high ^{227}Ac flux. Epping et al. (2002) showed that the geochemistry of the Nazaré Canyon sediments may be significantly affected by benthic macrofauna activity. Margin sediments are thus likely a source of ^{227}Ac to the water column. In particular, station 1 is located on the Iberian margin; the high $^{227}Ac_{ex}$ activity found at relatively shallow depth could result from a lateral input of ^{227}Ac released by the shallow sediments deposited onto the margin, a signal that is then be advected toward offshore waters, thus reaching station 13 and station 21 via different paths (Barbot et al., 2022). Near the Iberian margin (station 1), transmissiometry data indicate a shallow nepheloid layer

(10 [illegible] es, Barbot et al. (2022) established that internal tides (ITs) generated in the Bay of Biscay and along the Iberian slope could facilitate sediment resuspension and could be the major mechanism for the resuspension happening below 300 m. As hypothesized for bottom waters, we cannot exclude that the shallow nepheloid layers impact the distribution of radionuclides such as Ra or ^{227}Ac (Fig.4); in some cases, these nepheloid layers may act as a sink when particles scavenge chemical elements (e.g., radionuclides), while in other cases, they may act as a source when chemical elements are released from the particles.

4.4. Estimate of vertical eddy diffusivity coefficients (K_z)

When the vertical profiles of ^{227}Ac result from the diffusion of ^{227}Ac from the sediment and are not impacted by any other input or removal (e.g., bottom nepheloid layer), the vertical profiles of $^{227}Ac_{ex}$ activities can be used to derive vertical eddy diffusivity coefficients K_z (Nozaki, 1984). Vertical eddy diffusivity coefficients can be determined using a simplified vertical one-dimension model, assuming steady state conditions and that the impact of advection can be neglected (Nozaki, 1984):

$$\frac{\partial}{\partial z}\left(K_z \frac{\partial A}{\partial z}\right) - \lambda A = 0 \qquad \text{Equation 2}$$

Where K_z is the vertical eddy diffusivity coefficient; A is the $^{227}Ac_{ex}$ activity; z is the depth above the bottom; λ is the ^{227}Ac decay constant.

The solution of Equation 2 is given by:

$$A = A_0 e^{\left(-\sqrt{\frac{\lambda}{K_z}} z\right)} \qquad \text{Equation 3}$$

Where $A=A_0$ at z=0 and A=0 at $z \to \infty$.

We applied this equation at station 13 located in the Iberian Abyssal Plain (Fig.6).

Station 13 was selected because it is the deepest station (5455 m) of the section and it displays significant $^{227}Ac_{ex}$ activities (up to 0.42 dpm m^{-3}) near the seafloor. We do not observe a bottom nepheloid layer at this station (Fig.4), as it was the case at several other stations where we cannot exclude that resuspended Mn oxides may impact ^{227}Ac activities near the seafloor. The K_z value derived from the vertical profile of $^{227}Ac_{ex}$ is 0.68 ±0.49 cm^2 s^{-1} at that station (Fig.6). This value is within the lower range of K_z values usually reported for the deep ocean (0.1–50 cm^2 s^{-1};Huh and Ku, 1998; Kaufman et al., 1973; Koch-Larrouy et al., 2015; Nozaki, 1984; Nozaki et al., 1990). This low K_z can be explained by the topography of the Iberian Abyssal Plain since vertical mixing is linked to the underlying bathymetry and especially seafloor roughness (Polzin et al., 1997; Mauritzen et al., 2002). In

the [illegible] Ridge compared to the interior of the basins (Hasumi and Suginohara, 1999; Mauritzen et al., 2002).

Conclusion

This study reports an oceanic section of ^{227}Ac activities built from 9 full-depth vertical profiles determined between Portugal and Canada in the North Atlantic. By combining the ^{227}Ac activities with the ^{231}Pa activities, we provide an entire section of $^{227}Ac_{ex}$ activities. ^{227}Ac activities were relatively low along that section compared to other oceanic regions (e.g., Pacific Ocean). In most cases, ^{227}Ac was in secular equilibrium with ^{231}Pa. This suggests that at these depths, ^{227}Ac was only produced from the decay of ^{231}Pa in the water column and that there was no external input - younger than ~100 years - of ^{227}Ac. East of the section, the vertical ^{227}Ac and ^{231}Pa activities increased with increasing depth, a pattern that can be explained by both the origin and age of the deep waters in the West European Basin that drove the ^{231}Pa activities (reversible exchange model). West of the section, the presence of recently ventilated (young) water masses leads to low and relatively uniform ^{227}Ac and ^{231}Pa activities throughout the water column.

Below 2000 m, several vertical profiles were characterized by higher $^{227}Ac_{ex}$ activities near the seafloor, which reflect the input of ^{227}Ac that diffused out of the sediment. Sporadic enrichments of $^{227}Ac_{ex}$ were observed either in surface/subsurface or deep waters, which could be attributed to waters that interacted with the margins. At station 44 in the Irminger Basin, the high $^{227}Ac_{ex}$ activities at 2500 m were accompanied by high DFe concentrations; these two enrichments may indicate the presence of a hydrothermal plume. Finally, bottom nepheloid layers were observed along the section. High PMn concentrations were found in these layers and may contribute to scavenging radionuclides such as ^{227}Ac (and ^{226}Ra), a process that may impact the vertical profiles of $^{227}Ac_{ex}$ (and Ra). At station 13 (Iberian Abyssal Plain), where no bottom nepheloid layer was observed, we estimated a vertical eddy diffusivity coefficient (K_z) of 0.67±0.14 cm^2 s^{-1} from the ^{227}Ac vertical distribution; this value is consistent with K_z values previously documented for the deep ocean.

Figure 1: Location of stations investigated for ^{227}Ac (and ^{231}Pa) along the GEOVIDE section (GEOTRACES GA01). Surface currents are displayed in warm colors while deeper currents are displayed in cold colors.

Figure 2: Distribution of salinity (CTD data) along the GEOVIDE section. The different water masses are indicated (MW: Mediterranean Water, LSW: Labrador Sea Water, NEADWl: Lower North East Atlantic Deep Water, ISOW: Iceland-Scotland Overflow Water, DSOW: Denmark Strait Overflow Water). The station numbers are found on top of the figure. The sampling depths for ^{227}Ac are shown for each vertical profile (black dots). The isohalines are represented (white lines). This section was created with Ocean Data View (2022).

Figure 3: Distribution of dissolved ^{227}Ac activities along the GEOVIDE section with the dissolved ^{231}Pa activities (dpm m^{-3}) in contours. Station numbers are found on top of the panel. The sampling depths for ^{227}Ac are shown for each vertical profile (black dots). This section was created with Ocean Data View (2022).

Figure 4: Vertical profiles of dissolved ^{227}Ac with ^{231}Pa, ^{27}Ac$_{ex}$, ^{226}Ra, DFe, PMn and transmissiometry determined along the GEOVIDE section. Note that the scale may be different from one station to the other. The seafloor is represented by the bottom line. Nepheloid layers are represented by the shaded area. DFe and PMn concentrations are reported in Tonnard et al. (2018) and Gourain et al. (2018), respectively and are available in the GEOTRACES Intermediate Data Product (2021). This section was created with Ocean Data View (2022).

Figure 5: Distribution of dissolved ^{227}Ac$_{ex}$ activities along the GEOVIDE section. Station numbers are found on top of the panel. The sampling depths for ^{227}Ac are shown for each vertical profile (black dots).

Figure 6: Vertical profiles of ^{227}Ac$_{ex}$ activities (dpm m^{-3}) determined at station 13 in the last 1500 m. The exponential fit used to estimate the vertical eddy diffusivity (Kz in cm^2 s^{-1}) is shown (red line) with the interval of possible values (dashed grey lines).

Table 1: Activities of ^{227}Ac, and ^{227}Ac$_{ex}$ along the GEOVIDE section.

Station	Longitude (°E)	Latitude (°N)	Depth (m)	^{227}Ac (dpm m^{-3})	^{227}Ac$_{ex}$ (dpm m^{-3})
1	-10.04	40.33	45	0.13 ± 0.02	0.08 ± 0.03
1	-10.04	40.33	170	0.06 ± 0.01	0.00 ± 0.01
1	-10.04	40.33	350	0.06 ± 0.01	-0.01 ± 0.02
1	-10.04	40.33	500	0.30 ± 0.05	0.21 ± 0.06
1	-10.04	40.33	550	0.13 ± 0.02	0.04 ± 0.03
1	-10.04	40.33	800	0.11 ± 0.02	0.00 ± 0.03
1	-10.04	40.33	1050	0.11 ± 0.02	-0.01 ± 0.03
1	-10.04	40.33	2000	0.14 ± 0.03	-0.03 ± 0.03
1	-10.04	40.33	2500	0.20 ± 0.04	-0.01 ± 0.05
1	-10.04	40.33	3000	0.20 ± 0.04	-0.04 ± 0.05
1	-10.04	40.33	3450	0.14 ± 0.03	0.13 ± 0.04
13	-13.89	41.38	4	0.27 ± 0.05	0.21 ± 0.05
13	-13.89	41.38	40	0.10 ± 0.02	0.05 ± 0.02
13	-13.89	41.38	170	0.13 ± 0.02	0.07 ± 0.03
13	-13.89	41.38	350	0.10 ± 0.02	0.03 ± 0.02
13	-13.89	41.38	450	0.11 ± 0.02	0.05 ± 0.03
13	-13.89	41.38	1500	0.07 ± 0.01	-0.09 ± 0.03
13	-13.89	41.38	3000	0.19 ± 0.03	-0.05 ± 0.05
13	-13.89	41.38	4000	0.14 ± 0.03	-0.10 ± 0.04
13	-13.89	41.38	4850	0.29 ± 0.05	0.08 ± 0.06
13	-13.89	41.38	5280	0.65 ± 0.12	0.42 ± 0.12
21	-19.67	46.54	4	0.00 ± 0.00	-0.06 ± 0.01
21	-19.67	46.54	300	0.03 ± 0.01	-0.03 ± 0.01
21	-19.67	46.54	450	0.16 ± 0.03	0.09 ± 0.03
21	-19.67	46.54	800	0.07 ± 0.01	-0.02 ± 0.02
21	-19.67	46.54	1500	0.04 ± 0.01	-0.07 ± 0.02
21	-19.67	46.54	2700	0.08 ± 0.02	0.00 ± 0.02
21	-19.67	46.54	3500	0.17 ± 0.03	-0.04 ± 0.04
21	-19.67	46.54	3944	0.17 ± 0.03	-0.05 ± 0.04
21	-19.67	46.54	4444	0.31 ± 0.06	0.05 ± 0.07
26	-22.60	50.28	1013	0.09 ± 0.02	0.02 ± 0.02

26	-22.60	50.28	3563	0.14 ± 0.03	-0.05 ± 0.04
26	-22.60	50.28	3868	0.44 ± 0.08	0.23 ± 0.09
26	-22.60	50.28	4126	0.29 ± 0.05	0.16 ± 0.06
32	-26.71	55.51	4	0.18 ± 0.03	0.08 ± 0.03
32	-26.71	55.51	450	0.09 ± 0.02	-0.01 ± 0.02
32	-26.71	55.51	800	0.06 ± 0.01	-0.04 ± 0.02
32	-26.71	55.51	1481	0.10 ± 0.02	-0.03 ± 0.03
32	-26.71	55.51	2267	0.07 ± 0.01	-0.02 ± 0.02
32	-26.71	55.51	2854	0.08 ± 0.02	-0.02 ± 0.02
32	-26.71	55.51	3050	0.21 ± 0.04	0.09 ± 0.04
32	-26.71	55.51	3170	0.18 ± 0.03	0.07 ± 0.04
38	-31.27	58.84	100	0.09 ± 0.02	-0.04 ± 0.02
38	-31.27	58.84	297	0.02 ± 0.00	-0.11 ± 0.02
38	-31.27	58.84	643	0.12 ± 0.02	-0.05 ± 0.03
38	-31.27	58.84	840	0.08 ± 0.01	-0.02 ± 0.02
38	-31.27	58.84	1087	0.08 ± 0.01	-0.03 ± 0.02
38	-31.27	58.84	1235	0.15 ± 0.03	0.00 ± 0.03
38	-31.27	58.84	1316	0.07 ± 0.01	-0.09 ± 0.03
44	-38.95	59.62	4	0.14 ± 0.03	0.05 ± 0.02
44	-38.95	59.62	500	0.14 ± 0.03	0.03 ± 0.03
44	-38.95	59.62	1136	0.06 ± 0.01	-0.03 ± 0.02
44	-38.95	59.62	1972	0.09 ± 0.02	-0.05 ± 0.03
44	-38.95	59.62	2560	1.12 ± 0.21	1.00 ± 0.21
44	-38.95	59.62	2746	0.06 ± 0.01	-0.01 ± 0.02
44	-38.95	59.62	2880	0.17 ± 0.03	0.08 ± 0.03
64	-46.08	59.07	40	0.16 ± 0.03	0.06 ± 0.03
64	-46.08	59.07	400	0.13 ± 0.02	0.04 ± 0.03
64	-46.08	59.07	900	0.07 ± 0.01	-0.05 ± 0.02
64	-46.08	59.07	1372	0.13 ± 0.02	0.05 ± 0.03
64	-46.08	59.07	1716	0.09 ± 0.02	-0.03 ± 0.02
64	-46.08	59.07	2060	0.21 ± 0.04	0.11 ± 0.04
64	-46.08	59.07	2313	0.08 ± 0.02	-0.02 ± 0.02
64	-46.08	59.07	2443	0.29 ± 0.05	0.20 ± 0.05
69	-48.09	55.84	460	0.08 ± 0.01	0.01 ± 0.02
69	-48.09	55.84	1778	0.13 ± 0.02	0.01 ± 0.03
69	-48.09	55.84	2463	0.31 ± 0.06	0.25 ± 0.06
69	-48.09	55.84	2953	0.11 ± 0.03	0.08 ± 0.03
69	-48.09	55.84	3440	0.23 ± 0.04	0.17 ± 0.04
69	-48.09	55.84	3616	0.12 ± 0.02	0.08 ± 0.02
77	-51.09	52.99	4	0.27 ± 0.05	0.16 ± 0.05
77	-51.09	52.99	4	0.08 ± 0.02	-0.02 ± 0.00
77	-51.09	52.99	643	0.03 ± 0.01	-0.06 ± 0.01

Acknowledgement

Emilie Le Roy's fellowship was co-funded by the European Union and the Région Occitanie-Pyrénées-Méditerranée (European Regional Development Fund). The GEOVIDE project was co-funded by the French national program LEFE/INSU (GEOVIDE), ANR Blanc (GEOVIDE, ANR-13-BS06-0014) and RPDOC (ANR-12-PDOC-0025-01), LabEX MER (ANR-10-LABX-19) and IFREMER. M.A.C. was

sup[illegible] and crew of the N/O *Pourquoi Pas?*. The GEOVIDE cruise would not have been achieved without the technical skills and commitment of Catherine Kermabon, Olivier Ménage, Stéphane Leizour, Michel Hamon, Philippe Le Bot, Emmanuel de Saint-Léger and Fabien Pérault. We acknowledge Frédéric Planchon, Hélène Planquette, Yi Tang, Maxi Castrillejo, Nolwenn Lemaître and Catherine Jeandel for their help during ISP deployment and sampling. We would like to thank co-chief scientists Pascale Lherminier and Géraldine Sarthou. We acknowledge also Doug Hammond and an anonymous reviewer for their constructive comments.

van Aken, H. M.: The hydrography of the mid-latitude northeast Atlantic Ocean. I: The deep water masses, Deep-Sea Res. Part I, 47, 757–788, https://doi.org/10.1016/S0967-0637(99)00092-8, 2000.

Anderson, R. F., Bacon, M. P., and Brewer, P. G.: Removal of 230Th and 231Pa at ocean margins, Earth Planet. Sci. Lett., 66, 73–90, https://doi.org/10.1016/0012-821X(83)90127-9, 1983.

Bacon, M. P., Spencer, D. W., and Brewer, P. G.: 210Pb/226Ra and 210Po/210Pb disequilibria in seawater and suspended particulate matter, Earth Planet. Sci. Lett., 32, 277–296, https://doi.org/10.1016/0012-821X(76)90068-6, 1976.

Barbot, S., Lagarde, M., Lyard, F., Marsaleix, P., Lherminier, P., and Jeandel, C.: Internal Tides Responsible for Lithogenic Inputs Along the Iberian Continental Slope, J. Geophys. Res. Oceans, 127, e2022JC018816, https://doi.org/10.1029/2022JC018816, 2022.

Deng, F., Henderson, G. M., Castrillejo, M., and Perez, F. F.: Evolution of 231Pa and 230Th in overflow waters of the North Atlantic, Biogeosciences Discuss, 2018, 1–24, https://doi.org/10.5194/bg-2018-191, 2018.

Dulaiova, H., Sims, K. W. W., Charette, M. A., Prytulak, J., and Blusztajn, J. S.: A new method for the determination of low-level actinium-227 in geological samples, J. Radioanal. Nucl. Chem., 296, 279–283, https://doi.org/10.1007/s10967-012-2140-0, 2012.

Epping, E., van der Zee, C., Soetaert, K., and Helder, W.: On the oxidation and burial of organic carbon in sediments of the Iberian margin and Nazaré Canyon (NE Atlantic), Prog. Oceanogr., 52, 399–431, https://doi.org/10.1016/S0079-6611(02)00017-4, 2002.

García-Ibáñez, M. I., Pardo, P. C., Carracedo, L. I., Mercier, H., Lherminier, P., Ríos, A. F., and Pérez, F. F.: Structure, transports and transformations of the water masses in the Atlantic Subpolar Gyre, Prog. Oceanogr., 135, 18–36, https://doi.org/10.1016/j.pocean.2015.03.009, 2015.

García-Ibáñez, M. I., Pérez, F. F., Lherminier, P., Zunino, P., Mercier, H., and Tréguer, P.: Water mass distributions and transports for the 2014 GEOVIDE cruise in the North Atlantic, Biogeosciences, 15, 2075–2090, https://doi.org/10.5194/bg-15-2075-2018, 2018.

Geibert, W. and Vöge, I.: Progress in the determination of 227Ac in sea water, Mar. Chem., 109, 238–249, https://doi.org/10.1016/j.marchem.2007.07.012, 2008.

Geibert, W., Rutgers van der Loeff, M. M., Hanfland, C., and Dauelsberg, H.-J.: Actinium-227 as a deep-sea tracer: sources, distribution and applications, Earth Planet. Sci. Lett., 198, 147–165, https://doi.org/10.1016/S0012-821X(02)00512-5, 2002.

Geibert, W., Charette, M. A., Kim, G., Moore, W. S., Street, J. H., Young, M., and Paytan, A.: Dissolved actinium in the ocean, https://doi.org/10.1594/PANGAEA.695909, 2008.

GEOTRACES Intermediate Data Product Group: The GEOTRACES Intermediate Data Product 2021 (IDP2021). (1), https://doi.org/10.5285/CF2D9BA9-D51D-3B7C-E053-8486ABC0F5FD, 2021.

German, C. R. and Parson, L. M.: Distributions of hydrothermal activity along the Mid-Atlantic Ridge:

int[illegible]41, https://doi.org/10.1016/S0012-821X(98)00093-4, 1998.

Ghaleb, B., Pons-Branchu, E., and Deschamps, P.: Improved method for radium extraction from environmental samples and its analysis by thermal ionization mass spectrometry, J. Anal. At. Spectrom., 19, 906–910, https://doi.org/10.1039/B402237H, 2004.

Giffin, C., Kaufman, A., and Broecker, W.: Delayed coincidence counter for the assay of actinon and thoron, J. Geophys. Res., 68, 1749–1757, https://doi.org/10.1029/JZ068i006p01749, 1963.

Gourain, A., Planquette, H., Cheize, M., Lemaitre, N., Menzel Barraqueta, J.-L., Shelley, R., Lherminier, P., and Sarthou, G.: Inputs and processes affecting the distribution of particulate iron in the North Atlantic along the GEOVIDE (GEOTRACES GA01) section, Biogeosciences Discuss, 2018, 1–42, https://doi.org/10.5194/bg-2018-234, 2018.

Haskell, W. Z., Kadko, D., Hammond, D. E., Knapp, A. N., Prokopenko, M. G., Berelson, W. M., and Capone, D. G.: Upwelling velocity and eddy diffusivity from ^{7}Be measurements used to compare vertical nutrient flux to export POC flux in the Eastern Tropical South Pacific, Mar. Chem., 168, 140–150, https://doi.org/10.1016/j.marchem.2014.10.004, 2015.

Hasumi, H. and Suginohara, N.: Effects of locally enhanced vertical diffusivity over rough bathymetry on the world ocean circulation, J. Geophys. Res. Oceans, 104, 23367–23374, https://doi.org/10.1029/1999JC900191, 1999.

Henderson, P., Morris, P., Moore, W., and Charette, M.: Methodological advances for measuring low-level radium isotopes in seawater, J. Radioanal. Nucl. Chem., 296, 357–362, https://doi.org/10.1007/s10967-012-2047-9, 2013.

Huh, C.-A. and Ku, T.-L.: A 2—D section of 228Ra and 226Ra in the Northeast Pacific, Oceanol. Acta, 21, 533–542, https://doi.org/10.1016/S0399-1784(98)80036-4, 1998.

Jenkins, W. J., Doney, S. C., Fendrock, M., Fine, R., Gamo, T., Jean-Baptiste, P., Key, R., Klein, B., Lupton, J. E., Newton, R., Rhein, M., Roether, W., Sano, Y., Schlitzer, R., Schlosser, P., and Swift, J.: A comprehensive global oceanic dataset of helium isotope and tritium measurements, Earth Syst. Sci. Data, 11, 441–454, https://doi.org/10.5194/essd-11-441-2019, 2019.

Kaufman, A., Trier, R. M., Broecker, W. S., and Feely, H. W.: Distribution of 228Ra in the world ocean, J. Geophys. Res., 78, 8827–8848, https://doi.org/10.1029/JC078i036p08827, 1973.

Kemnitz, N., Hammond, D. E., Henderson, P., Le Roy, E., Charette, M., Moore, W., Anderson, R. F., Fleisher, M. Q., Leal, A., Black, E., Hayes, C. T., Adkins, J., Berelson, W., and Bian, X.: Actinium and radium fluxes from the seabed in the northeast Pacific Basin, Mar. Chem., 104180, https://doi.org/10.1016/j.marchem.2022.104180, 2022.

Kipp, L. E., Charette, M. A., Hammond, D. E., and Moore, W. S.: Hydrothermal vents: A previously unrecognized source of actinium-227 to the deep ocean, Mar. Chem., 177, Part 4, 583–590, https://doi.org/10.1016/j.marchem.2015.09.002, 2015.

Souhaut, M.: Estimates of tidal mixing in the Indonesian archipelago from multidisciplinary INDOMIX in-situ data, Deep Sea Res. Part Oceanogr. Res. Pap., 106, 136–153, https://doi.org/10.1016/j.dsr.2015.09.007, 2015.

Ku, T.-L., Knauss, K. G., and Mathieu, G. G.: Uranium in open ocean: concentration and isotopic composition, Deep Sea Res., 24, 1005–1017, https://doi.org/10.1016/0146-6291(77)90571-9, 1977.

Lacan, F. and Jeandel, C.: Neodymium isotopic composition and rare earth element concentrations in the deep and intermediate Nordic Seas: Constraints on the Iceland Scotland Overflow Water signature, Geochem. Geophys. Geosystems, 5, 2004.

Lacan, F. and Jeandel, C.: Acquisition of the neodymium isotopic composition of the North Atlantic Deep Water, Geochem. Geophys. Geosystems, 6, Q12008, https://doi.org/10.1029/2005GC000956, 2005.

Lazier, J. R. N.: The renewal of Labrador sea water, Deep Sea Res. Oceanogr. Abstr., 20, 341–353, https://doi.org/10.1016/0011-7471(73)90058-2, 1973.

Le Roy, E., Sanial, V., Lacan, F., van Beek, P., Souhaut, M., Charette, M. A., and Henderson, P. B.: Insight into the measurement of dissolved 227Ac in seawater using radium delayed coincidence counter, Mar. Chem., S0304420318302536, https://doi.org/10.1016/j.marchem.2019.04.002, 2019.

Levier, M., Roy-Barman, M., Colin, C., and Dapoigny, A.: Determination of low level of actinium 227 in seawater and freshwater by isotope dilution and mass spectrometry, Mar. Chem., 233, 103986, https://doi.org/10.1016/j.marchem.2021.103986, 2021.

Mauritzen, C., Polzin, K. L., McCartney, M. S., Millard, R. C., and West-Mack, D. E.: Evidence in hydrography and density fine structure for enhanced vertical mixing over the Mid-Atlantic Ridge in the western Atlantic, J. Geophys. Res. Oceans, 107, 11-1-11–19, https://doi.org/10.1029/2001JC001114, 2002.

McCartney, M. S.: Recirculating components to the deep boundary current of the northern North Atlantic, Prog. Oceanogr., 29, 283–383, 1992.

Moore, W. S. and Arnold, R.: Measurement of 223Ra and 224Ra in coastal waters using a delayed coincidence counter, J. Geophys. Res. Oceans, 101, 1321–1329, https://doi.org/10.1029/95JC03139, 1996.

Nozaki, Y.: Excess 227Ac in deep ocean water, Nature, 310, 486–488, https://doi.org/10.1038/310486a0, 1984.

Nozaki, Y.: Actinium-227: A Steady State Tracer for the Deep-sea Basin-wide Circulation and Mixing Studies, in: Elsevier Oceanography Series, vol. 59, edited by: Teramoto, T., Elsevier, 139–156, https://doi.org/10.1016/S0422-9894(08)71323-0, 1993.

Nozaki, Y., Yamada, M., and Nikaido, H.: The marine geochemistry of actinium-227: Evidence for its migration through sediment pore water, Geophys. Res. Lett., 17, 1933–1936,

Nozaki, Y., Yamada, M., Nakanishi, T., Nagaya, Y., Nakamura, K., Shitashima, K., and Tsubota, H.: The distribution of radionuclides and some trace metals in the water columns of the Japan and Bonin trenches, Oceanol. Acta, 21, 469–484, https://doi.org/10.1016/S0399-1784(98)80031-5, 1998.

Polzin, K. L., Toole, J. M., Ledwell, J. R., and Schmitt, R. W.: Spatial Variability of Turbulent Mixing in the Abyssal Ocean, Science, 276, 93–96, https://doi.org/10.1126/science.276.5309.93, 1997.

Read, J. F.: CONVEX-91: water masses and circulation of the Northeast Atlantic subpolar gyre, Prog. Oceanogr., 48, 461–510, https://doi.org/10.1016/S0079-6611(01)00011-8, 2000.

Ocean Data View: https://odv.awi.de/, last access: 15 November 2022.

Schmitz, W. J. and McCartney, M. S.: On the North Atlantic Circulation, Rev. Geophys., 31, 29–49, https://doi.org/10.1029/92RG02583, 1993.

Swarzenski, P. W. and Baskaran, M.: Is the extraction of thorium onto MnO2-coated filter cartridges uniform?, U.S. Geological Survey, 2004.

Tonnard, M., Planquette, H., Bowie, A. R., Merwe, P. van der, Gallinari, M., Desprez de Gésincourt, F., Germain, Y., Gourain, A., Benetti, M., Reverdin, G., Tréguer, P., Boutorh, J., Cheize, M., Menzel Barraqueta, J.-L., Pereira-Contreira, L., Shelley, R., Lherminier, P., and Sarthou, G.: Dissolved iron in the North Atlantic Ocean and Labrador Sea along the GEOVIDE section (GEOTRACES section GA01), Biogeosciences Discuss., 1–53, https://doi.org/10.5194/bg-2018-147, 2018.

Yashayaev, I. and Dickson, B.: Transformation and Fate of Overflows in the Northern North Atlantic, in: Arctic–Subarctic Ocean Fluxes, edited by: Dickson, R. R., Meincke, J., and Rhines, P., Springer Netherlands, 505–526, https://doi.org/10.1007/978-1-4020-6774-7_22, 2008.

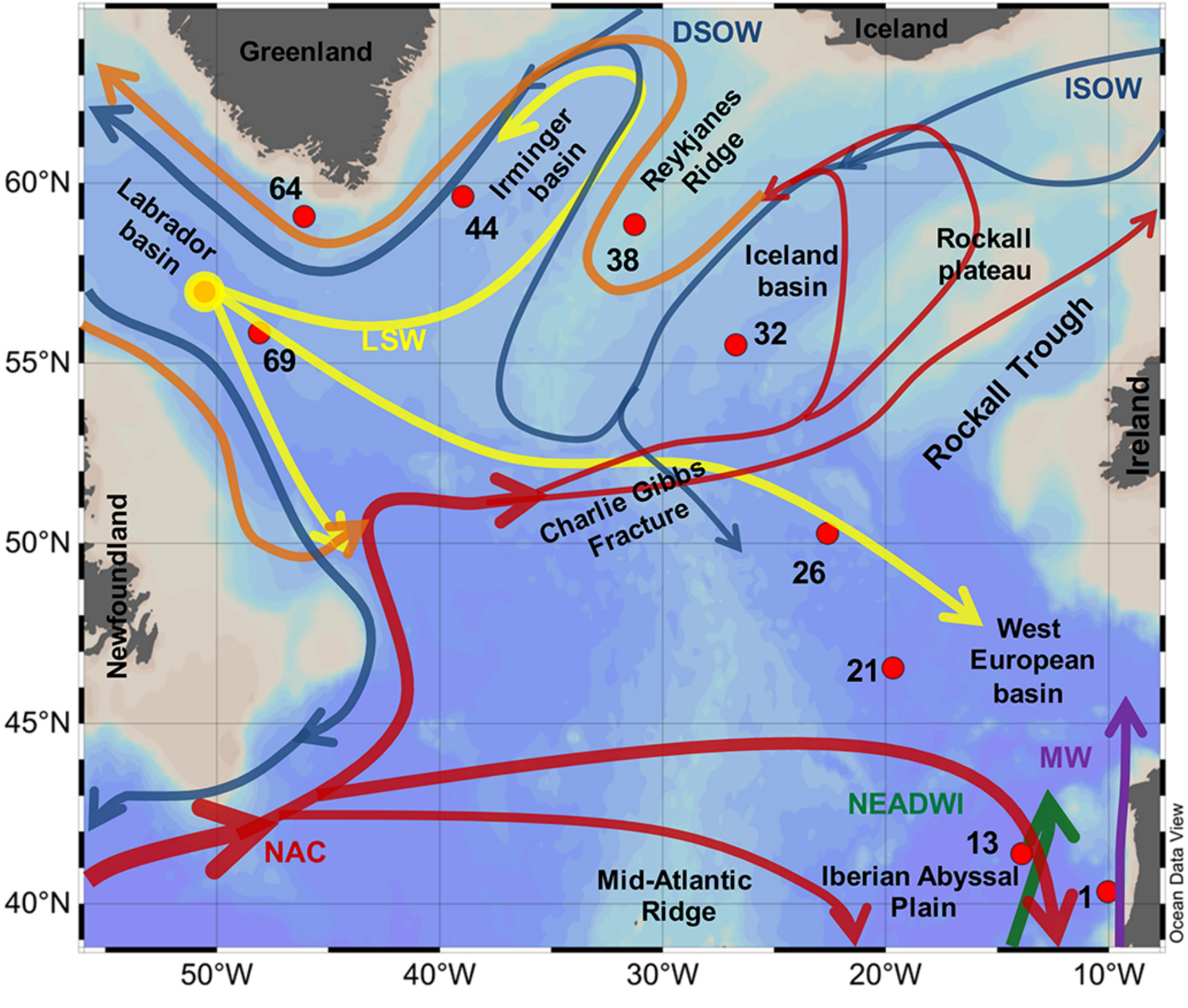
Greenland
Iceland
DSOW
ISOW
Irminger basin
Reykjanes Ridge
Labrador basin
64
44
38
Iceland basin
Rockall plateau
LSW
69
32
Rockall Trough
Ireland
Charlie Gibbs Fracture
Newfoundland
26
West European basin
21
MW
NEADWI
NAC
13
Mid-Atlantic Ridge
Iberian Abyssal Plain
1
60°N
55°N
50°N
45°N
40°N
50°W
40°W
30°W
20°W
10°W
Ocean Data View

Figure 1

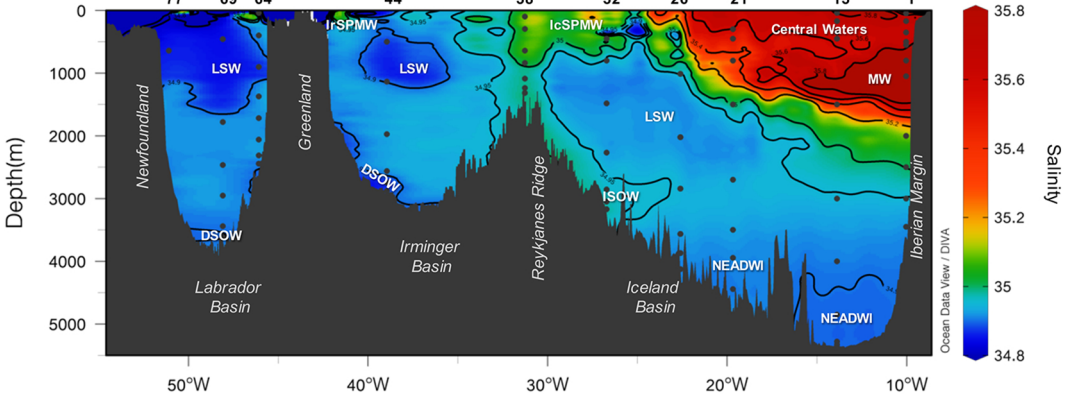
77
69
64
44
38
32
26
21
13
1
0
1000
2000
3000
4000
5000
Depth(m)
LSW
IrSPMW
LSW
IcSPMW
Central Waters
MW
LSW
Newfoundland
Greenland
DSOW
DSOW
ISOW
Reykjanes Ridge
Iberian Margin
Irminger
Basin
Labrador
Basin
Iceland
Basin
NEADWI
NEADWI
50°W
40°W
30°W
20°W
10°W
Ocean Data View / DIVA
35.8
35.6
35.4
35.2
35
34.8
Salinity

Figure 2

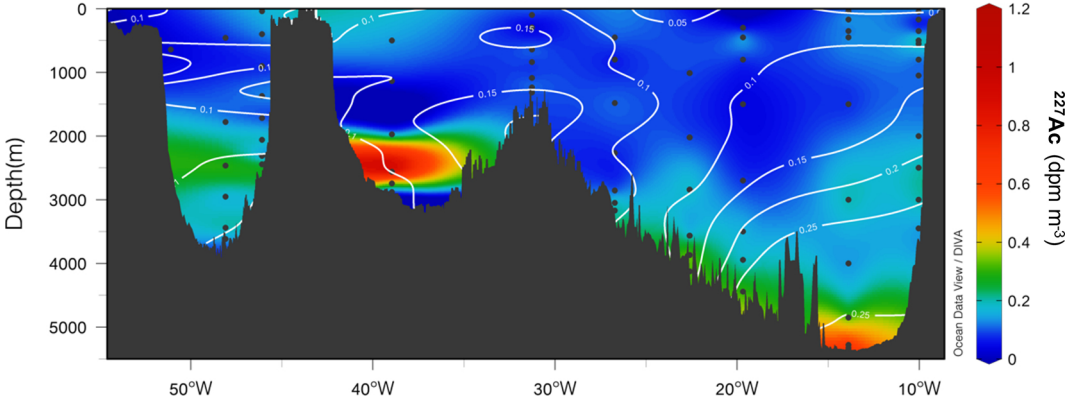
77
69
64
44
38
32
26
21
13
1
Depth(m)
0
1000
2000
3000
4000
5000
50°W
40°W
30°W
20°W
10°W
0.1
0.15
0.05
0.2
0.25
Ocean Data View / DIVA
227Ac (dpm m-3)
1.2
1
0.8
0.6
0.4
0.2
0

Figure 3

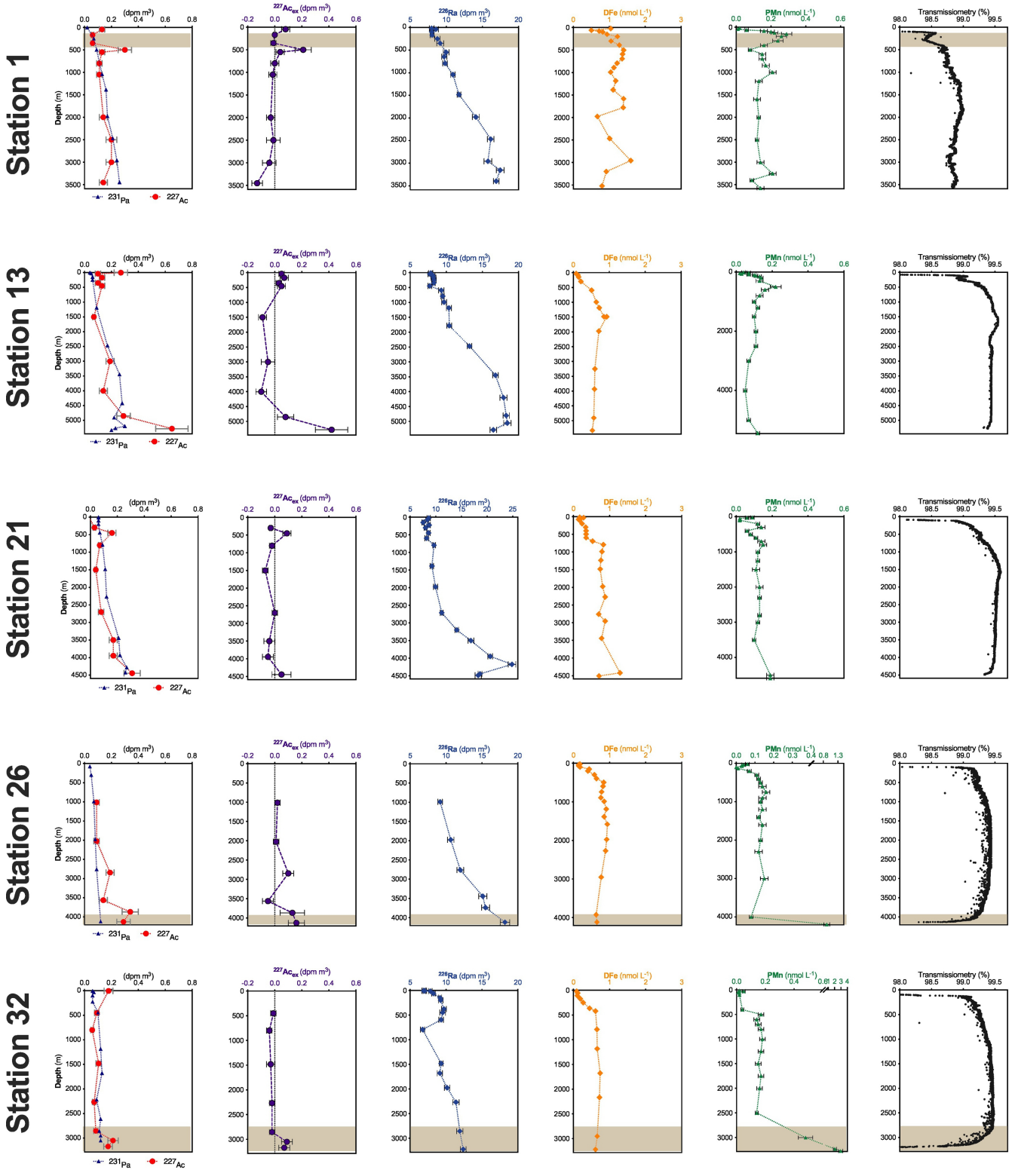
Station 1
Station 13
Station 21
Station 26
Station 32
Depth (m)
(dpm m³)
231Pa
227Ac
227Ac_ex (dpm m³)
226Ra (dpm m³)
DFe (nmol L⁻¹)
PMn (nmol L⁻¹)
Transmissiometry (%)

Figure 4a

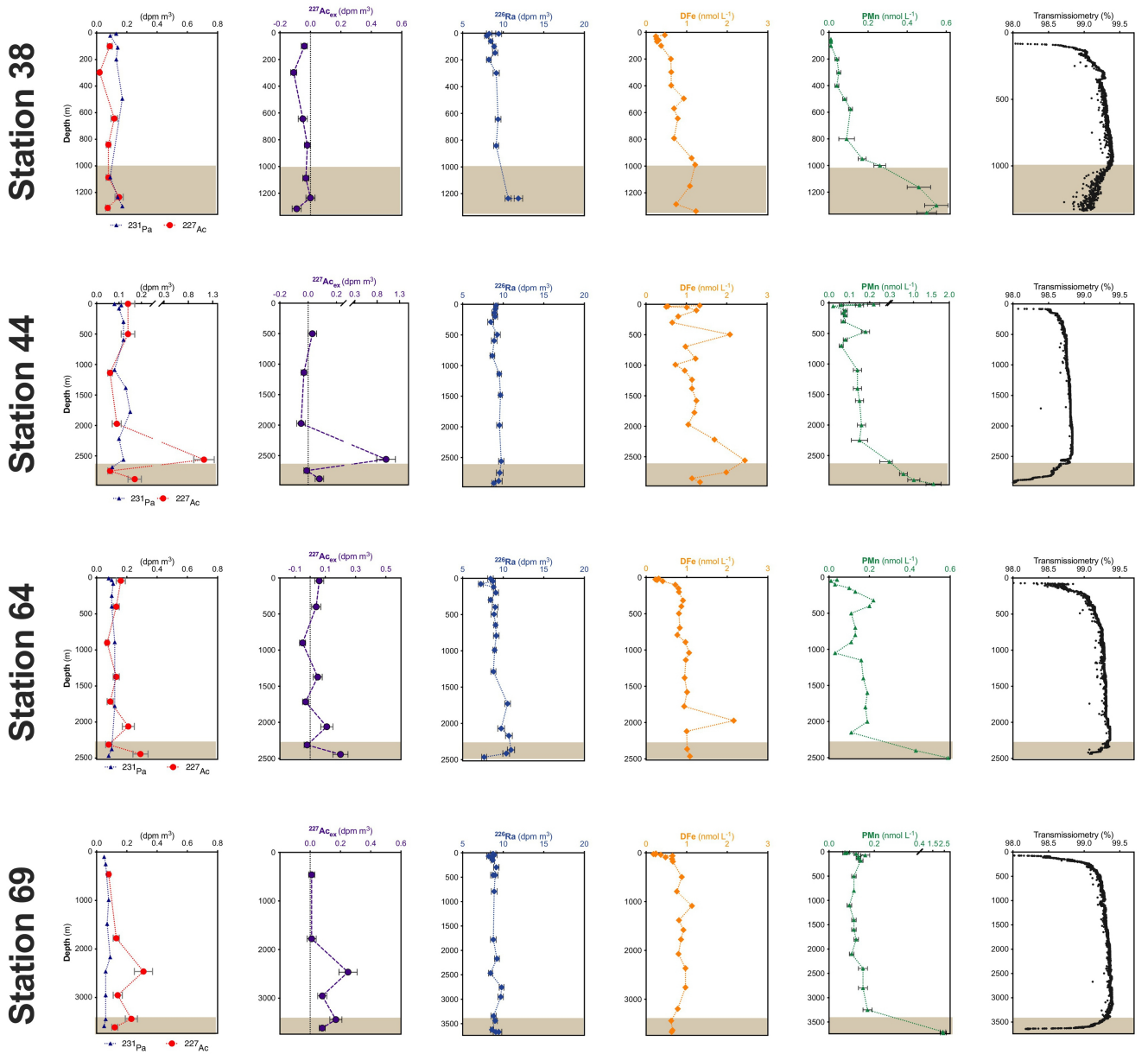
Station 38
Station 44
Station 64
Station 69
Depth (m)
(dpm m3)
231Pa
227Ac
227Acex (dpm m3)
226Ra (dpm m3)
DFe (nmol L-1)
PMn (nmol L-1)
Transmissiometry (%)

Figure 4b

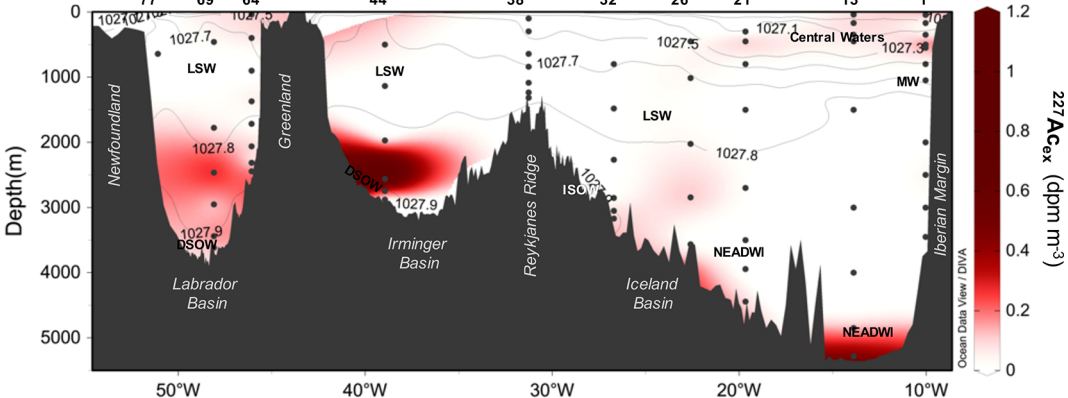
77
69
64
44
38
32
26
21
13
1
Depth(m)
0
1000
2000
3000
4000
5000
50°W
40°W
30°W
20°W
10°W
Newfoundland
Greenland
Reykjanes Ridge
Iberian Margin
Labrador Basin
Irminger Basin
Iceland Basin
LSW
DSOW
ISOW
NEADWI
MW
Central Waters
1027.1
1027.3
1027.5
1027.7
1027.8
1027.9
Ocean Data View / DIVA
$^{227}Ac_{ex}$ (dpm m^{-3})
1.2
1
0.8
0.6
0.4
0.2
0

Figure 5

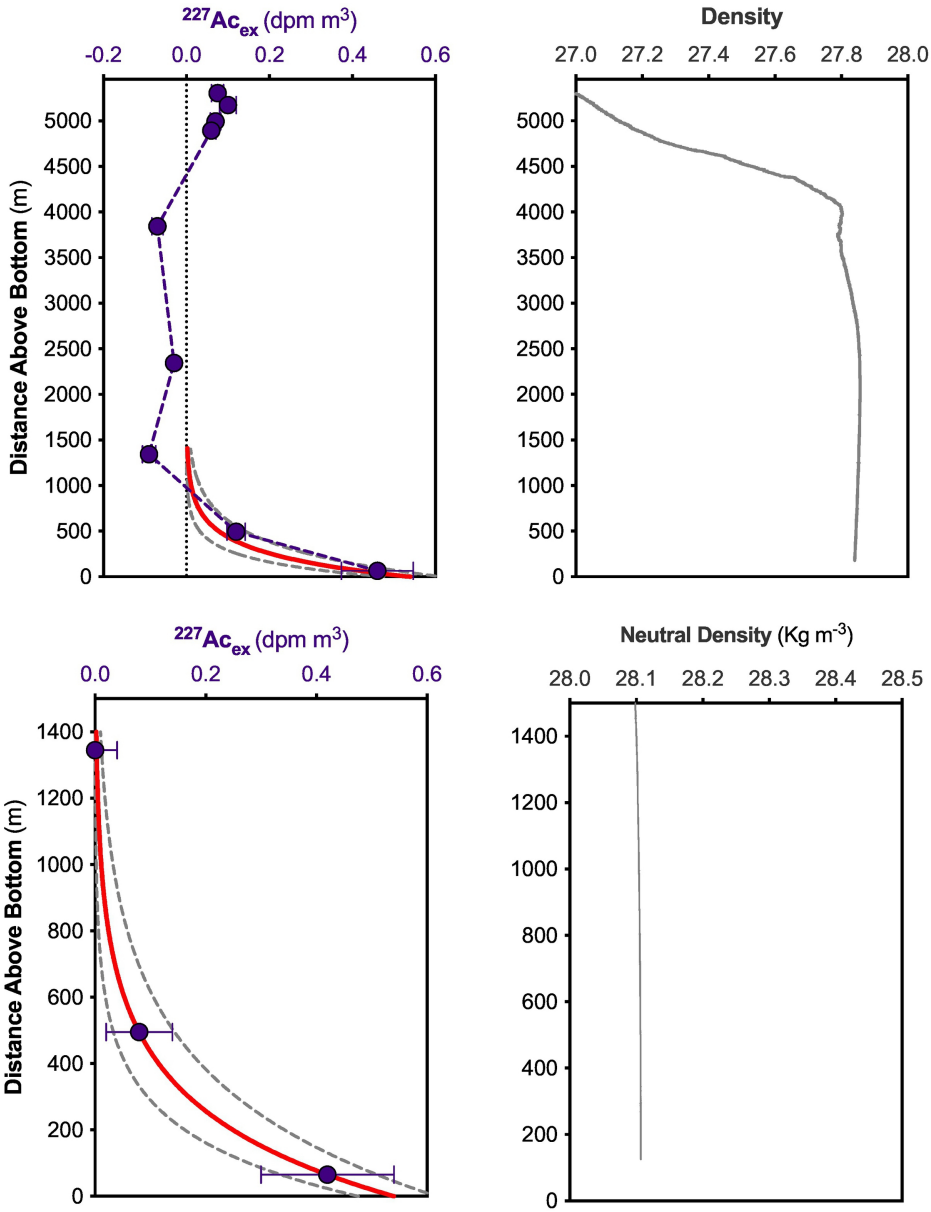
$^{227}Ac_{ex}$ (dpm m^3)
-0.2
0.0
0.2
0.4
0.6
Distance Above Bottom (m)
5000
4500
4000
3500
3000
2500
2000
1500
1000
500
0
Density
27.0
27.2
27.4
27.6
27.8
28.0
$^{227}Ac_{ex}$ (dpm m^3)
0.0
0.2
0.4
0.6
Distance Above Bottom (m)
1400
1200
1000
800
600
400
200
0
Neutral Density (Kg m^{-3})
28.0
28.1
28.2
28.3
28.4
28.5

Figure 6